frontiers in Chemistry

ORIGINAL RESEARCH
published: 12 July 2021
doi: 10.3389/fchem.2021.713078

# Hypochlorite-Activated Fluorescence Emission and Antibacterial Activities of Imidazole Derivatives for Biological Applications

*Thanh Chung Pham[1], Van-Nghia Nguyen[2], Yeonghwan Choi[1], Dongwon Kim[3], Ok-Sang Jung[3], Dong Joon Lee[4], Hak Jun Kim[5], Myung Won Lee[5], Juyoung Yoon[2], Hwan Myung Kim[4,6]* and Songyi Lee[1,5]**

[1]Industry 4.0 Convergence Bionics Engineering, Pukyong National University, Busan, South Korea, [2]Department of Chemistry and Nanoscience, Ewha Womans University, Seoul, South Korea, [3]Department of Chemistry, Pusan National University, Busan, South Korea, [4]Department of Energy Systems Research, Ajou University, Suwon, South Korea, [5]Department of Chemistry, Pukyong National University, Busan, South Korea, [6]Department of Chemistry, Ajou University, Suwon, South Korea

The ability to detect hypochlorite (HOCl/$ClO^-$) *in vivo* is of great importance to identify and visualize infection. Here, we report the use of imidazoline-2-thione (**$R_1SR_2$**) probes, which act to both sense $ClO^-$ and kill bacteria. The $N_2C{=}S$ moieties can recognize $ClO^-$ among various typical reactive oxygen species (ROS) and turn into imidazolium moieties (**$R_1IR_2$**) *via* desulfurization. This was observed through UV–vis absorption and fluorescence emission spectroscopy, with a high fluorescence emission quantum yield ($\Phi_F$ = 43–99%) and large Stokes shift (Δν~115 nm). Furthermore, the **DIM** probe, which was prepared by treating the **DSM** probe with $ClO^-$, also displayed antibacterial efficacy toward not only *Escherichia coli* (*E. coli*) and *Staphylococcus aureus* (*S. aureus*) but also methicillin-resistant *Staphylococcus aureus* (MRSA) and extended-spectrum ß-lactamase–producing *Escherichia coli* (ESBL-EC), that is, antibiotic-resistant bacteria. These results suggest that the **DSM** probe has great potential to carry out the dual roles of a fluorogenic probe and killer of bacteria.

**Keywords: fluorescent sensor, fluorogenic probe, hypochlorite sensor, antibacterial effect, probe–killer**

OPEN ACCESS

***Edited by:***
*Dokyoung Kim,*
*Kyung Hee University, South Korea*

***Reviewed by:***
*Ki Tae Kim,*
*Chungbuk National University, South Korea*
*Daniel Gryko,*
*Polish Academy of Sciences, Poland*

****Correspondence:***
*Hwan Myung Kim*
*kimhm@ajou.ac.kr*
*Songyi Lee*
*slee@pknu.ac.kr*

***Specialty section:***
*This article was submitted to Chemical Biology, a section of the journal Frontiers in Chemistry*

***Received:*** *21 May 2021*
***Accepted:*** *17 June 2021*
***Published:*** *12 July 2021*

***Citation:***
*Pham TC, Nguyen V-N, Choi Y, Kim D, Jung O-S, Lee DJ, Kim HJ, Lee MW, Yoon J, Kim HM and Lee S (2021) Hypochlorite-Activated Fluorescence Emission and Antibacterial Activities of Imidazole Derivatives for Biological Applications. Front. Chem. 9:713078. doi: 10.3389/fchem.2021.713078*

## INTRODUCTION

Invasion of microorganisms such as bacteria and viruses can cause infectious diseases. Due to the worldwide increase in cases of severe bacterial diseases, scientists have attempted to develop technologies that serve as both fluorogenic probes for the identification of infection and antibacterial agents. Unfortunately, the continued overuse of antibiotics coupled with the rapid spread of resistance mechanisms has rendered many antibiotics inactive (Kardas et al., 2005). As a result, new pathogens have come into being that are multidrug resistant (MDR), such as methicillin-resistant *Staphylococcus aureus* (MRSA) and extended-spectrum ß-lactamase–producing *Escherichia coli* (ESBL-EC), which have undermined most clinically useful antibiotics. Therefore, the emergence of drug-resistant bacteria is one of the growing challenges to anti-infection therapy. At the same time, emerging infectious diseases need very urgent and immediate treatment due to their rapid spread. In this regard, theragnostics, a treatment strategy that combines therapeutics with diagnostics, could be embraced by clinicians and patients (Pene et al., 2009). In recent years, material-based approaches have found preliminary use for the treatment of bacterial infections (Kurapati et al., 2016; Gupta

et al., 2019) and for the image-guided treatment of bacterial infections (Kim et al., 2018; Lee S. et al., 2020). Such methods have provided an approach that can produce the desired therapeutic effect with a reduced potential to develop drug-resistant bacteria (Lee et al., 2016; Li et al., 2018a; Li et al., 2018b; Li et al., 2019). Among the various reactive oxygen species (ROS), hypochlorite ($HOCl/ClO^-$) acts as a powerful microbicidal agent in the innate immune system. $ClO^-$ is mainly produced by the myeloperoxidase (MPO)-catalyzed reaction of $H_2O_2$ and $Cl^-$ in immunocytes (Domigan et al., 1995; Xu et al., 2013; Pak et al., 2018; Wu et al., 2019; Nguyen et al., 2020). The regulated production of microbicidal HOCl is required for the host to control invading microbes. On the other hand, $OCl^-$ reacts rapidly with a variety of biomolecules and is connected with various disorders (Winterbourn et al., 2000; Krasowska and Konat, 2004; Jeitner et al., 2005).

A fundamentally important yet challenging feature of studies in this area is the design of new chemorecognition processes. Imidazolium salts with good water solubility and stability have been used as fluorescence sensors in aqueous solution (Xu et al., 2010; Kim et al., 2012; Xu et al., 2015). To take advantage of the properties of imidazolium salts, we designed imidazoline-2-thione ($\mathbf{R_1SR_2}$) probes to be $ClO^-$ fluorescent probes capable of inducing bacterial growth inhibition. Furthermore, the photophysical properties of $\mathbf{R_1IR_2}$ and $\mathbf{R_1SR_2}$ were examined *via* not only experimental results but also time-dependent DFT (TD-DFT) calculation. Bacterial growth was significantly reduced by the imidazolium moieties ($\mathbf{R_1IR_2}$) that were generated by the treatment of $\mathbf{R_1SR_2}$ with $ClO^-$. Among the pairs of $\mathbf{R_1IR_2}$ and $\mathbf{R_1SR_2}$, the **DSM** probe showed excellent selectivity and sensitivity toward $ClO^-$. Also, the **DIM** probe showed antibacterial efficacy toward not only *E. coli* and *S. aureus* but also methicillin-resistant *S. aureus* (MRSA) and extended-spectrum ß-lactamase–producing *E. coli* (ESBL-EC). The **DIM** probe initially induces electrostatic interactions between the cationic imidazolium salts and the negatively charged bacterial surface, followed by structural perturbation, resulting in bacterial cell death. Similar membrane disruption through interactions of cationic imidazolium groups has been suggested by previous reports (Riduan and Zhang, 2013). Overall, this report demonstrates the importance and benefits of the new fluorogenic probe **DSM** for anti-pathogenic diagnostic and therapeutic applications.

## EXPERIMENTAL DESIGN

For the synthesis of $\mathbf{R_1SR_2}$, a mixture of $\mathbf{R_1IR_2}$ (0.1 mmol), sulfur (1.0 mmol), and sodium methoxide (1.0 mmol) in anhydrous methanol (20 ml) was stirred overnight at room temperature. After the solvent was removed, the crude product was dissolved in DW and extracted by MC 3 times. The organic phase was collected and dried over $Na_2SO_4$. It was purified by silica gel column chromatography, using H/MC (9/1) as the eluent to get a white solid as the product (yield ~90%).

**BSB**: $^1$H NMR (400 MHz, chloroform-*d*) δ 7.77 (dd, *J* = 6.3, 3.3 Hz, 2H), 7.69–7.61 (m, 2H), 7.41–7.32 (m, 4H), 7.20–7.09 (m, 4H), 6.97–6.90 (m, 2H), 5.80 (s, 4H). $^{13}$C NMR (101 MHz, chloroform-*d*) δ 174.85, 134.28, 133.18, 131.93, 130.55, 129.36, 128.02, 127.84, 127.82, 125.25, 122.77, 105.92, 48.67. ESI HRMS m/z = 536.9630 $[M + H]^+$, calc. for $C_{25}H_{18}Br_2N_2S$ = 535.96.

**BSM**: $^1$H NMR (400 MHz, chloroform-*d*) δ 7.92–7.85 (m, 1H), 7.81–7.73 (m, 1H), 7.67–7.59 (m, 1H), 7.53 (s, 1H), 7.40 (pd, *J* = 6.8, 1.6 Hz, 2H), 7.31 (s, 1H), 7.16–7.06 (m, 2H), 6.89–6.81 (m, 1H), 5.73 (s, 2H), 3.93 (d, *J* = 0.6 Hz, 3H). $^{13}$C NMR (101 MHz, chloroform-*d*) δ 174.26, 134.36, 133.07, 132.92, 131.88, 130.53, 130.46, 129.24, 127.94, 127.86, 127.83, 127.70, 125.21, 125.09, 122.67, 105.70, 105.04, 48.35, 31.68. ESI HRMS m/z = 383.0212 $[M + H]^+$, calc. for $C_{19}H_{15}BrN_2S$ = 382.01.

**CSB**: $^1$H NMR (400 MHz, chloroform-*d*) δ 8.04 (dt, *J* = 7.8, 0.9 Hz, 2H), 7.75 (d, *J* = 7.5 Hz, 2H), 7.62 (dd, *J* = 7.7, 1.6 Hz, 1H), 7.48–7.33 (m, 6H), 7.24–7.17 (m, 4H), 7.08 (dtd, *J* = 16.7, 7.4, 1.7 Hz, 2H), 6.82–6.75 (m, 1H), 5.69 (s, 2H), 4.42 (td, *J* = 6.8, 2.1 Hz, 4H), 2.06 (dq, *J* = 31.4, 7.4 Hz, 4H). $^{13}$C NMR (101 MHz, chloroform-*d*) δ 140.43, 133.08, 129.23, 127.94, 127.75, 125.82, 125.11, 122.99, 120.51, 119.03, 108.77, 105.76, 105.04, 77.42, 77.10, 76.78, 48.33, 44.73, 42.65. ESI HRMS m/z = 612.1080 $[M + Na]^+$, calc. for $C_{34}H_{28}BrN_3S$ = 589.12.

**CSC**: $^1$H NMR (400 MHz, chloroform-*d*) δ 8.03 (dt, *J* = 7.9, 1.0 Hz, 4H), 7.74 (dd, *J* = 6.3, 3.3 Hz, 2H), 7.46–7.35 (m, 10H), 7.23–7.13 (m, 6H), 4.34 (dt, *J* = 18.7, 6.8 Hz, 8H), 2.10–2.00 (m, 4H), 1.94 (q, *J* = 7.2 Hz, 4H), 1.30–1.20 (m, 4H), 0.90–0.79 (m, 4H). $^{13}$C NMR (101 MHz, chloroform-*d*) δ 172.90, 140.42, 131.88, 130.15, 127.69, 125.78, 124.96, 122.97, 120.49, 119.00, 108.77, 104.90, 77.42, 77.11, 76.79, 44.41, 42.64, 26.09, 25.31. ESI HRMS m/z = 665.2709 $[M + Na]^+$, calc. for $C_{43}H_{38}N_4S$ = 642.28.

**CSD**: $^1$H NMR (600 MHz, chloroform-*d*) δ 8.03 (dt, *J* = 7.7, 1.0 Hz, 2H), 7.79 (d, *J* = 1.9 Hz, 1H), 7.75 (ddd, *J* = 8.1, 2.2, 1.2 Hz, 2H), 7.45–7.37 (m, 6H), 7.23–7.16 (m, 5H), 6.67–6.64 (m, 1H), 5.61 (s, 2H), 4.41 (q, *J* = 7.0 Hz, 4H), 2.14–1.96 (m, 4H). $^{13}$C NMR (101 MHz, chloroform-*d*) δ 173.81, 140.41, 135.38, 133.57, 131.64, 131.14, 130.29, 128.96, 127.78, 127.72, 125.82, 125.22, 123.16, 122.99, 121.99, 120.52, 119.05, 108.74, 105.56, 105.20, 77.42, 77.11, 76.79, 47.86, 44.76, 42.64, 26.05, 25.29. ESI HRMS m/z = 690.0185 $[M + Na]^+$, calc. for $C_{34}H_{27}Br_2N_3S$ = 667.03.

**CSM**: $^1$H NMR (400 MHz, chloroform-*d*) δ 8.04 (dt, *J* = 7.7, 1.0 Hz, 2H), 7.74 (dd, *J* = 6.6, 3.0 Hz, 2H), 7.62 (dd, *J* = 7.7, 1.5 Hz, 1H), 7.48–7.33 (m, 6H), 7.26 (s, 7H), 7.24–7.15 (m, 4H), 7.08 (dtd, *J* = 16.7, 7.4, 1.7 Hz, 2H), 6.78 (dd, *J* = 7.4, 1.9 Hz, 1H), 5.69 (s, 2H), 4.42 (dd, *J* = 7.3, 5.7 Hz, 4H), 2.10 (p, *J* = 6.8 Hz, 2H), 2.01 (p, *J* = 7.0 Hz, 2H). $^{13}$C NMR (101 MHz, chloroform-*d*) δ 173.25, 140.43, 132.81, 131.89, 130.28, 127.79, 127.63, 125.78, 125.03, 124.94, 122.96, 120.48, 119.00, 108.78, 104.91, 104.80, 44.47, 42.65, 31.31, 26.12, 25.38. ESI HRMS m/z = 458.1661 $[M + Na]^+$, calc. for $C_{28}H_{25}N_3S$ = 435.18.

**DSB**: $^1$H NMR (400 MHz, chloroform-*d*) δ 7.84–7.73 (m, 3H), 7.69–7.60 (m, 1H), 7.43–7.34 (m, 3H), 7.33 (s, 1H), 7.31–7.22 (m, 3H), 7.20–7.09 (m, 2H), 6.96–6.89 (m, 1H), 6.82 (dd, *J* = 8.3, 0.8 Hz, 1H), 5.79 (s, 2H), 5.73 (s, 2H). $^{13}$C NMR (101 MHz, chloroform-*d*) δ 174.80, 135.49, 134.20, 133.54, 133.21, 131.87, 131.74, 131.22, 130.60, 130.54, 129.41, 129.08, 128.02, 127.84, 127.79, 125.38, 123.27, 122.78, 122.13, 106.09, 105.72, 48.70, 48.21. ESI HRMS m/z = 614.8735 $[M + H]^+$, calc. for $C_{25}H_{17}Br_3N_2S$ = 613.87.

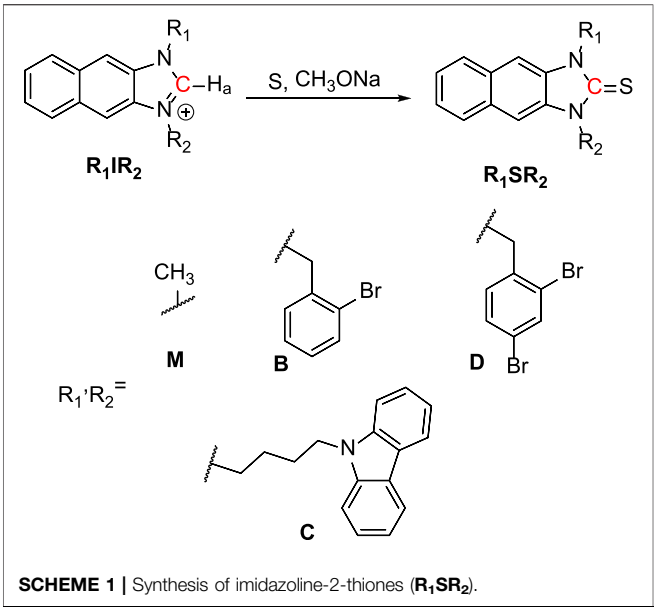


**SCHEME 1 |** Synthesis of imidazoline-2-thiones (**$R_1SR_2$**).

**DSD**: $^1$H NMR (400 MHz, chloroform-*d*) δ 7.84–7.74 (m, 4H), 7.40 (dd, *J* = 6.3, 3.2 Hz, 2H), 7.34 (s, 2H), 7.28 (dd, *J* = 8.3, 1.9 Hz, 2H), 6.80 (dd, *J* = 8.3, 0.7 Hz, 2H), 5.72 (s, 4H). $^{13}$C NMR (101 MHz, chloroform-*d*) δ 174.73, 135.53, 133.44, 131.67, 131.22, 130.59, 129.05, 127.82, 125.50, 123.29, 122.20, 105.89, 48.24. ESI HRMS m/z = 692.7840 $[M + H]^+$, calc. for $C_{25}H_{16}Br_4N_2S$ = 691.78.

**DSM**: $^1$H NMR (400 MHz, chloroform-*d*) δ 7.93–7.85 (m, 1H), 7.79 (dd, *J* = 7.5, 2.0 Hz, 2H), 7.53 (s, 1H), 7.48–7.36 (m, 2H), 7.28 (s, 1H), 7.22 (d, *J* = 2.0 Hz, 3H), 6.74 (dd, *J* = 8.3, 0.8 Hz, 1H), 5.66 (s, 2H), 3.92 (s, 3H). $^{13}$C NMR (101 MHz, chloroform-*d*) δ 174.15, 135.38, 133.61, 132.83, 131.65, 131.12, 130.56, 130.44, 129.07, 127.84, 127.73, 125.34, 125.24, 123.19, 122.01, 105.51, 105.22, 47.89, 31.71. ESI HRMS m/z = 460.9317 $[M + H]^+$, m/z = 482.9137 $[M+Na]^+$ calc. for $C_{19}H_{15}Br_2N_2S$ = 459.93.

## RESULTS AND DISCUSSION

### Molecular Design, Synthesis, and Characterization

As shown in **Scheme 1**, **$R_1IR_2$** was synthesized from 2,3-Diaminonaphthalene in a 3-step process as follows: imidazole cyclization, alkylation, and imidazolium salt formation. Several bromide and carbazole derivatives have shown antibacterial activity (Yaqub et al., 2013; Gottardi et al., 2014; Bashir et al., 2015; Liu et al., 2015; Salih et al., 2016; Popescu et al., 2021). Thus, the introduction of bromobenzyl, dibromobenzyl, and carbazole groups is expected to increase the antibacterial effect of the probes. Then, the **$R_1IR_2$** salt was treated with sulfur and $CH_3ONa$ as a catalyst in ACN, leading to the formation of the corresponding molecule **$R_1SR_2$**. All synthetic processes and collected structures are detailed in the experimental section and the supporting information. Several products were characterized not only by $^1$H NMR, $^1$C NMR, and HRMS spectra (**Supplementary Material**) but also by crystallization structures (**Figure 1**; **Supplementary Figures S37, S38**; **Supplementary Tables S1, S2**), which have not been reported in previous studies on similar $N_2C$=S structures (Xu et al., 2015; Xu et al., 2016). In particular, the length of the thioketone in the $N_2C$=S type was found to be 1.657–1.671 Å (**Table 1**), which is longer than that in other thioketone types such as thiobenzophenone, thioformaldehyde, thioacetone, etc. (~1.63–1.64 Å) due to the presence of C–N π-bonds (Mullen and Hellner, 1978; Allen et al., 1987). Thus, the $N_2C$=S bond can make the compound more active and sensitive toward ROS/RNS.

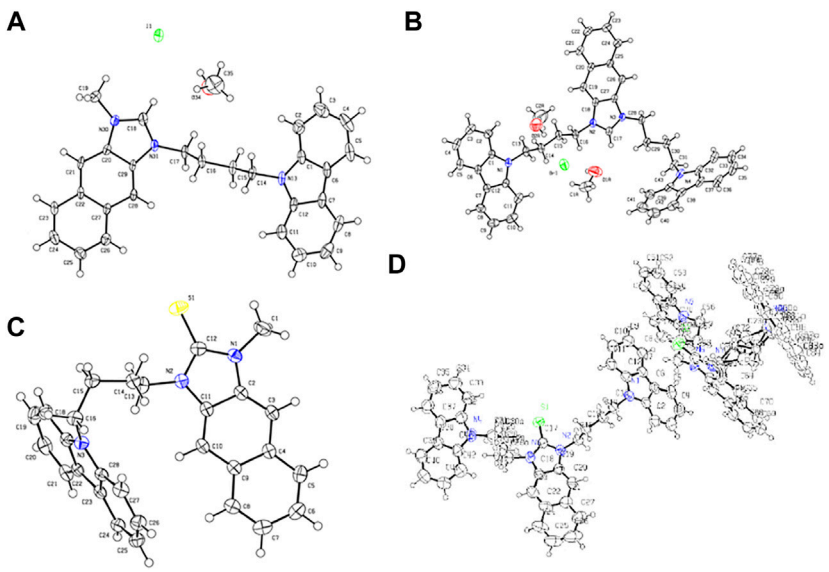


**FIGURE 1 |** Crystal structures of **(A) CIM**, **(B) CIC**, **(C) CSM**, and **(D) CSC**.

**TABLE 1 |** Bond lengths between the crystal and optimized structures of **CIM**, **CSM**, **CIC**, and **CSC**.

| Bond | CIM | | CSM | | CIC | | CSC | |
|---|---|---|---|---|---|---|---|---|
| | Crystal | Optimized | Crystal | Optimized | Crystal | Optimized | Crystal | Optimized |
| C=S | — | — | 1.671 Å | 1.669 Å | — | — | 1.657 Å | 1.670 Å |
| C-N/C=N | 1.332 | 1.333 Å | 1.367 Å | 1.381 Å | 1.329 Å | 1.334 Å | 1.383 Å | 1.380 Å |
| C-$H_a$ | 0.950 | 1.079 Å | — | — | 0.950 Å | 1.079 Å | — | — |

— *does not exist.*

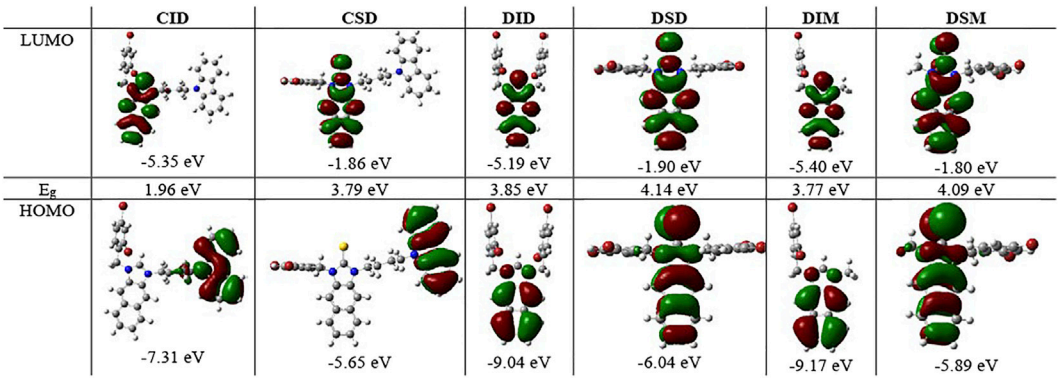


**FIGURE 2 |** Molecular orbitals and associated energies of **CID** and **CSD**, **DID** and **DSD**, **DIM** and **DSM**, and the energy gap ($E_g$) between the HOMO and the LUMO.

To better understand not only the molecular structures but also the molecular orbitals and energy levels of $\mathbf{R_1IR_2}$ and $\mathbf{R_1SR_2}$, geometrical optimization was performed through theoretical DFT calculations in the Gaussian 09 program package using the B3LVPs functional with the 6-31+g(2d,p) basis set (Pham et al., 2020). The optimized structures without imaginary frequencies were similar to the crystallization structures in terms of several critical bond lengths and angles (**Table 1**). Their molecular orbitals and energy levels from HOMO+2 to LUMO+2 are shown in **Supplementary Tables S1–S5**. The HOMO of $\mathbf{CIR_2}$ is located in the carbazole moiety, and the LUMO is located in the naphthalene–imidazolium salt center core. However, the HOMO and LUMO of $\mathbf{BIR_2}$ and $\mathbf{DIR_2}$ are concentrated in the naphthalene–imidazolium salt core (**Figure 2**). Similarly, the HOMO of $\mathbf{CSR_2}$ is located in the carbazole moiety, whereas the HOMO and LUMO of $\mathbf{BSR_2}$ and $\mathbf{DSR_2}$ are located in the naphthalene and imidazoline-2-thione moieties. The difference originates from the introduction of the carbazole moiety, which is known as a strong donor and fluorescence quencher (Ledwon, 2019; Rehmat et al., 2020; Saritha et al., 2020). Thus, the energy gap between the LUMO and the HOMO ($E_g$) of $\mathbf{CIR_2}$ (1.80–2.03 eV) is significantly lower than those of $\mathbf{BIR_2}$ and $\mathbf{DIR_2}$ (3.77–3.86 eV). The $E_g$ of $\mathbf{CSR_2}$ (3.79–3.86 eV) is lower than those of $\mathbf{BIR_2}$ and $\mathbf{DIR_2}$ (4.08–4.14 eV). The reduction in difference is assigned to the strong electron acceptor ability of imidazolium salts, which enhances electron transfer from the carbazole electron donor to the imidazolium salt electron acceptor (vs. from the carbazole to the naphthalene and imidazoline-2-thione moieties).

## Photophysical Properties and Theoretical Calculations

The UV–vis absorption and fluorescence emission spectroscopy of $\mathbf{R_1IR_2}$ and $\mathbf{R_1SR_2}$ were examined in various solvents (**Supplementary Figures S39–S47**). At the same time, time-dependent DFT (TD-DFT) calculations were carried out in the optimized structures using a hybrid functional method, a gradient-corrected method, and a popular local method (Adamo and Jacquemin, 2013; Pham et al., 2021a) to better understand their photophysical properties. The optical excitation energies of $\mathbf{R_1IR_2}$ and $\mathbf{R_1SR_2}$ were determined using the CAM-B3LYP functional with the Def-2-TZVP basis set and the TPSSTPSS functional with the 6-31+G (2 days, p) basis set, respectively. The results corresponded well to the experimental data. $\mathbf{R_1SR_2}$ showed absorption peaks at approximately 350 nm, with a high molar absorption coefficient ($\varepsilon = 31.4–62.8 \times 10^3$) and weak emission ($\Phi_F$ = 0.1–1.8%) (**Figure 3B**; **Table 2**). On the other hand, $\mathbf{R_1IR_2}$ exhibited absorption peaks at about 325 nm, with a lower molar absorption coefficient ($\varepsilon$ = 7.2–13.3 $\times 10^3$) (**Figure 3A**; **Table 2**). $\mathbf{R_1IR_2}$ without a carbazole moiety showed a strong emission peak at approximately 440 nm ($\Phi_F$ = 26–63%) and a large Stokes shift ($\Delta\nu \sim 115$ nm). In sharp contrast, $\mathbf{R_1IR_2}$ with a carbazole moiety exhibited weak emission ($\Phi_F$ = 3.8–8.2%) due to photoinduced electron transfer (PET) from the carbazole donor to the naphthalene–imidazolium salt acceptor (Sun et al., 2019). The absorption of $\mathbf{R_1IR_2}$ is assigned to the $S_0 \rightarrow S_1$ transition and its emission is assigned to the $S_1' \rightarrow S_0$ transition, with the orbital contribution located in the naphthalene–imidazolium salt core (**Supplementary Table**

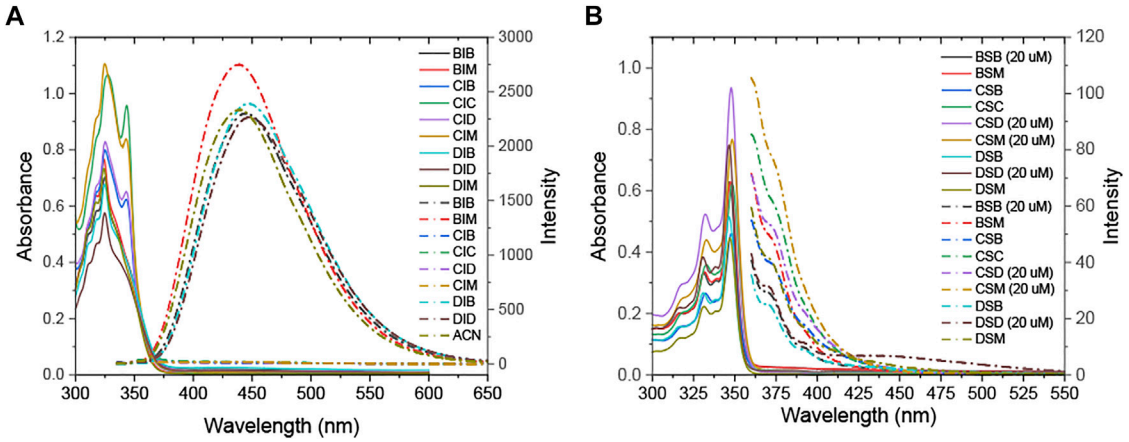


**FIGURE 3 |** UV–vis (solid line) and fluorescence emission (dashed/dotted line) spectra of **(A) $R_1IR_2$** (80 μM) and **(B) $R_1SR_2$** (10 μM) (in ACN).

**TABLE 2 |** Photophysical properties of **$R_1IR_2$** and **$R_1SR_2$** according to ACN and computational calculations.

| | $\lambda_{abs}$ (nm) | ε (× $10^3$) | $\lambda_{ems}$ (nm) | Δν (nm) | $\Phi_F$ (%) | $E_g$ (eV) | Absorption ($S_0 \rightarrow S_n$) | | | | Fluorescence ($S_n \rightarrow S_0$) | | |
|---|---|---|---|---|---|---|---|---|---|---|---|---|---|
| | | | | | | | $S_n$ | Orbital contribution | ΔE (eV) | f | $S_n$ | ΔE (eV) | f |
| **BIB** | 325 | 8.77 | 445 | 120 | 32.6 | 3.86 | $S_1$ | [H] → [L]: 96.3% | 3.954 | 0.12 | $S_1'$ | 3.463 | 0.22 |
| **BSB** | 347 | 31.42 | — | — | 0.8 | 4.12 | $S_3$ | [H-1] → [L]: 75.5% | 3.552 | 0.39 | $S_2'$ | 3.393 | 0.58 |
| **BIM** | 324 | 9.59 | 439 | 115 | 59.2 | 3.79 | $S_1$ | [H]→[L]: 96.4% | 3.955 | 0.12 | $S_1'$ | 3.508 | 0.23 |
| **BSM** | 348 | 62.75 | — | — | 0.9 | 4.08 | $S_3$ | [H-1] → [L]: 81.9% | 3.539 | 0.28 | $S_2'$ | 3.375 | 0.57 |
| **CIB** | 325 | 9.99 | 370 | 45 | 3.8 | 2.03 | $S_1$ | [H]→[L]: 95.9% | 3.942 | 0.13 | $S_1'$ | 3.482 | 0.23 |
| **CSB** | 353 | 54.45 | — | — | 1.1 | 3.84 | $S_6$ | [H-2] → [L]: 60.1% | 3.538 | 0.28 | $S_5'$ | 3.495 | 0.55 |
| **CIC** | 328 | 13.32 | 370 | 42 | 8.2 | 1.85 | $S_1$ | [H-4] → [L]: 95.5% | 3.932 | 0.16 | $S_1'$ | 3.335 | 0.22 |
| **CSC** | 349 | 62.16 | — | — | 0.9 | 3.81 | $S_{11}$ | [H-3] → [L]: 61.0% | 3.519 | 0.30 | $S_6'$ | 3.461 | 0.36 |
| **CID** | 325 | 10.36 | 370 | 45 | 5.1 | 1.96 | $S_1$ | [H-2] → [L]: 95.8% | 3.936 | 0.13 | $S_1'$ | 3.469 | 0.23 |
| **CSD** | 348 | 46.74 | — | — | 1.4 | 3.79 | $S_9$ | [H-2] → [L]: 66.7% | 3.540 | 0.27 | $S_3'$ | 3.638 | 0.53 |
| **CIM** | 325 | 13.82 | 371 | 46 | 4.6 | 1.80 | $S_1$ | [H-2] → [L]: 96.0% | 3.946 | 0.14 | $S_1'$ | 3.496 | 0.23 |
| **CSM** | 348 | 38.32 | — | — | 1.8 | 3.86 | $S_4$ | [H-1] → [L]: 56.5% | 3.502 | 0.29 | $S_4'$ | 3.451 | 0.65 |
| **DIB** | 325 | 8.46 | 446 | 121 | 26.4 | 3.86 | $S_1$ | [H]→[L]: 96.2% | 3.953 | 0.12 | $S_1'$ | 3.455 | 0.22 |
| **DSB** | 351 | 50.78 | — | — | 0.1 | 4.13 | $S_3$ | [H-1] → [L]: 71.7% | 3.550 | 0.36 | $S_2'$ | 3.401 | 0.57 |
| **DID** | 325 | 7.19 | 447 | 122 | 26.5 | 3.85 | $S_1$ | [H]→[L]: 96.1% | 3.947 | 0.12 | $S_1'$ | 3.449 | 0.22 |
| **DSD** | 347 | 37.41 | — | — | 0.1 | 4.14 | $S_3$ | [H-1] → [L]: 64.3% | 3.553 | 0.31 | $S_2'$ | 3.414 | 0.56 |
| **DIM** | 324 | 9.17 | 440 | 116 | 62.9 | 3.77 | $S_1$ | [H]→[L]: 96.3% | 3.950 | 0.12 | $S_1'$ | 3.484 | 0.22 |
| **DSM** | 347 | 44.56 | — | — | 0.1 | 4.09 | $S_3$ | [H-1] → [L]: 76.9% | 3.541 | 0.25 | $S_2'$ | 3.379 | 0.56 |

*The molar absorption coefficient (ε) ($M^{-1}$ $cm^{-1}$), stock shift (Δν), and fluorescence quantum yield ($\Phi_F$) were measured in DMSO and toluene for **$R_1IR_2$** and **$R_1SR_2$**, with 9,10-Diphenylanthracene ($\Phi_F$ = 0.90 in cyclohexane) being used as a reference; the oscillator strength (f), the energy gap ($E_g$) between the HOMO and LUMO levels, and the energy gap (ΔE) between $S_0$ and $S_n$/$S_n'$ were not observed.*

**S12**). **$R_1SR_2$** exhibited $S_0 \rightarrow S_3$ absorption and $S_2' \rightarrow S_1$ emission in the absence of carbazole groups, while it showed $S_0 \leftrightarrow S_n/S_n'$ transition at the higher level of $S_n/S_n'$ in the presence of carbazole groups. The absorption band is contributed by other orbitals in addition to the HOMO and the LUMO (**Supplementary Table S13**), but natural transition orbitals (NTOs) showed a similar electronic transition in the naphthalene and imidazoline-2-thione moieties of **$R_1SR_2$** (**Supplementary Table S14**), which demonstrates that the two have the same UV/vis absorption spectra (**Figure 3B**).

The fluorescence emission quantum yield of **BIM** and **DIM** ($\Phi_F$ = 59.2–62.9%) is significantly greater than that of **BIB**, **DIB**, and **DID** (26.4–32.6%) in DMSO, which is attributable to the absence or presence of the second (di)bromobenzyl group. The $S_1$ absorption energy of **BIB** and **BIM** vs. **DIB**, **DID**, and **DIM** is similar, whereas the $S_1'$ emission energy of **BIM** and **DIM** is higher than that of **BIB** and **DIB** or **DID**, respectively. Thus, the energy gap (ΔE) between the $S_1$ absorption and the $S_1'$ emission of **$R_1IM$** ($R_1$ = **B** or **D**) is lower than that of **$R_1IR_2$** ($R_1$, $R_2$ = **B** or **D**) (**Figure 4**). Moreover, the energy relaxation wastage of **$R_1IM$** ($R_1$ = **B** or **D**) from the $S_1$ absorption level to the $S_1'$ emission level is less than that of **$R_1IR_2$** (**$R_1$**, **$R_2$** = **B** or **D**), leading to the increase in fluorescence emission quantum yield of **BIM** and **DIM**.

At the different volume fractions of PBS buffer with a pH value of 7.4 (0–99.5%), the fluorescence emission of **DIM** and **DID** in DMF is maintained owing to the high water solubility of

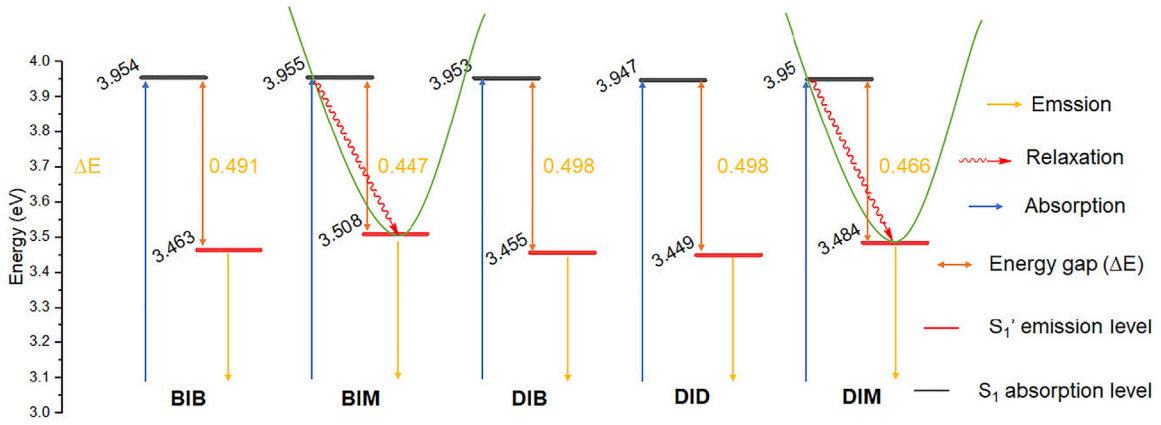


**FIGURE 4 |** Electronic energy levels diagram of **BIB**, **BIM**, **DIB**, **DID**, and **DIM**.

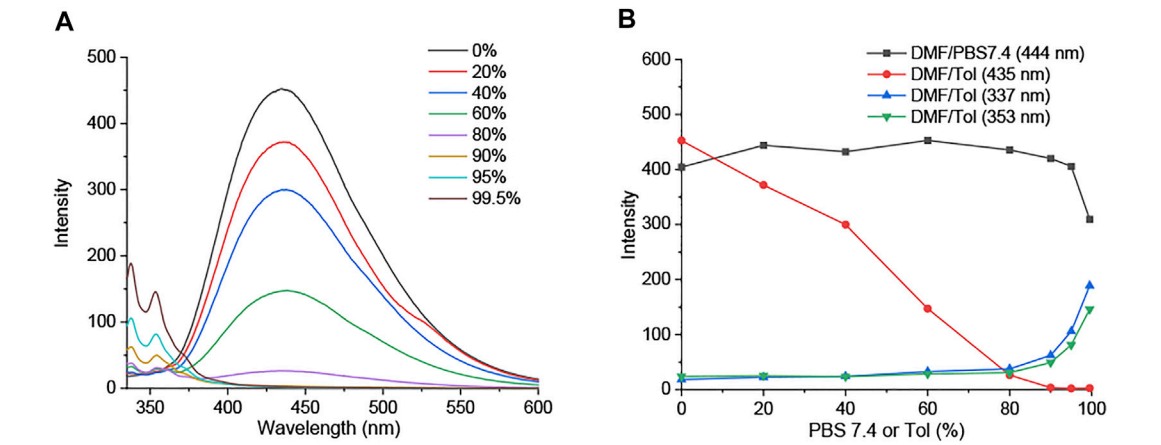


**FIGURE 5 | (A)** Fluorescence emission spectra of **DIM** (5 μM) in DMF/Tol (0–99.5%). **(B)** Fluorescence intensity at emission wavelength of **DIM** (5 μM) in DMF/PBS buffer (pH 7.4) and DMF/Tol (0–99.5%).

**TABLE 3 |** $CFU_{50}$ (μM) and *p*-value of $\mathbf{R_1IR_2}$ and $\mathbf{R_1SR_2}$ toward *E. coli*, *S. aureus*, ESBL-EC, EC-GFP, and MRSA bacteria ($CFU_{50(R1SR2)}$ > 128.0 μM).

| | *E. coli* | | *S. aureus* | | ESBL-EC | | EC-GFP | | MRSA | |
|---|---|---|---|---|---|---|---|---|---|---|
| | $CFU_{50}$ | *p*-value | $CFU_{50}$ | *p*-value | $CFU_{50}$ | *p*-value | $CFU_{50}$ | *p*-value | $CFU_{50}$ | *p*-value |
| BIB | 17.5 | > 7.3 | 3.3 | > 38.8 | 26.4 | > 4.8 | 19.8 | > 6.5 | 8.5 | > 15.1 |
| BIM | 45.3 | > 2.8 | 39.7 | > 3.2 | 53.0 | > 2.4 | 24.9 | > 5.1 | 15.2 | > 8.4 |
| CIB | > 128.0 | — | 2.4 | > 53.3 | > 128.0 | — | 21.4 | > 6.0 | 15.7 | > 8.2 |
| CIC | > 128.0 | — | 3.4 | > 37.6 | > 128.0 | — | 21.0 | > 6.1 | 15.7 | > 8.2 |
| CID | > 128.0 | — | 1.9 | > 67.4 | > 128.0 | — | 15.2 | > 8.4 | 14.6 | > 8.8 |
| CIM | 31.2 | > 4.1 | 4.2 | > 30.5 | 18.3 | > 7.0 | 11.9 | > 10.8 | 11.7 | > 10.9 |
| DIB | 9.5 | > 13.5 | 2.1 | > 60.1 | 8.7 | > 14.7 | 22.2 | > 5.8 | 4.1 | > 31.2 |
| DID | 11.1 | > 11.5 | 2.2 | > 58.2 | 14.0 | > 9.1 | 4.3 | > 29.8 | 5.4 | > 23.7 |
| DIM | 12.9 | > 9.9 | 6.0 | > 21.3 | 22.1 | > 5.8 | 14.9 | > 8.6 | 14.8 | > 8.6 |

—*not calculated.*

imidazolium salt groups (**Figure 5B**; **Supplementary Figures S48, S49**). We further examined their fluorescence emission in the aggregate state. Interestingly, the emission peak of **DIM** at 450 nm decreased, whereas a 335–350-nm emission band slightly increased with the increasing of toluene (Tol) concentration (0–99.5%) (**Figure 5A**). **DIM** showed the ACQ effect on its core structure

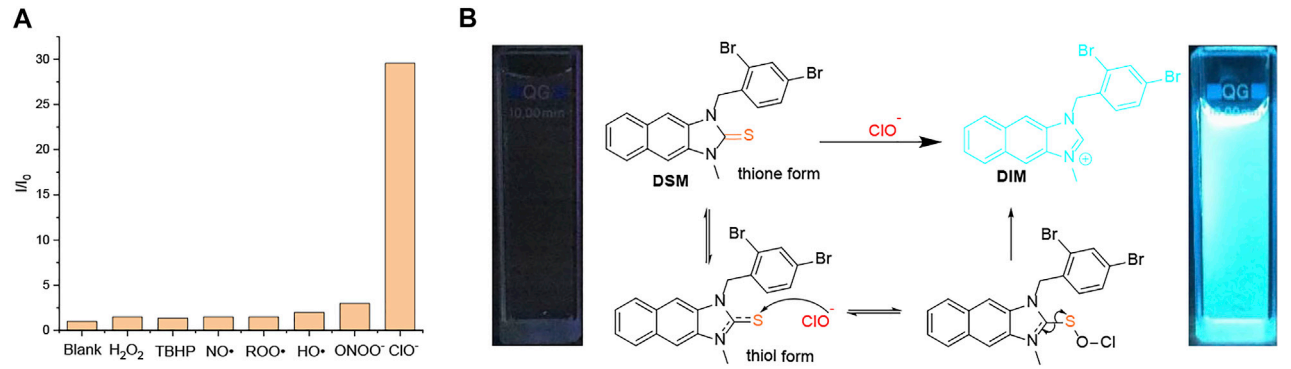


**FIGURE 6 | (A)** Fluorescence intensity ratio ($I/I_0$) of **DSM** (5 μM) in PBS buffer with a pH value of 7.4 (0.5% DMF) in the presence of $ClO^-$ (50 μM), $ROO^•$ (1 mM), $NO^•$ (1 mM), $H_2O_2$ (1 mM), TBHP (1 mM), $ONOO^-$ (200 μM), and •OH (200 μM). **(B)** Proposed desulfurization mechanism of **DSM** *via* hypochlorite ($ClO^-$).

in DMF being quenched in the high concentration of toluene (**Supplementary Figure S49**); at the same time, it showed blueshift emission assigned from the rotation of bromobenzyl groups around the imidazolium salt core.

## Antibacterial Activity

To compare the antibacterial activity of $\mathbf{R_1IR_2}$ and $\mathbf{R_1SR_2}$, we calculated the concentration (μM) ($CFU_{50}$) at which the CFU rate equals 50% and the $P=CFU_{50(R1IR2)}/CFU_{50(R1SR2)}$ between the imidazolium salt and imidazoline-2-thiones (**Table 3**). All $\mathbf{R_1SR_2}$ showed weak antibacterial ability toward *E. coli*, *S. aureus*, extended-spectrum ß-lactamase–producing *E. coli* (ESBL-EC), *E. coli* expressing green fluorescent protein (EC-GFP), and methicillin-resistant *S. aureus* (MRSA) bacteria with $CFU_{50}$ > 128.0 μM. In sharp contrast, almost all imidazolium salts ($\mathbf{R_1IR_2}$) exhibited a stronger antibacterial effect, including against ESBL-EC and MRSA ($p > 2.4$). The antibacterial efficiency of $\mathbf{R_1IR_2}$ is quite similar to that of dehydroepiandrosterone-derived (Hryniewicka et al., 2021), peptide-conjugated (Reinhardt et al., 2014), ethoxyether-functionalized (Huang et al., 2011), amino acid–derived (Valls et al., 2020), polydiacetylene-conjugated (Lee et al., 2016), and unsymmetrically substituted (Çoban et al., 2017; Duman et al., 2019) imidazolium salts in previous reports. Furthermore, the antibacterial activity of imidazolium salts ($\mathbf{R_1IR_2}$) increased following the substitution of methyl and bromobenzyl with dibromobenzyl groups and the change from one to two dibromobenzyl groups (**Table 3**).

On the other hand, the incorporation of dibromobenzyl groups enhanced the antibacterial effect toward Gram-positive bacteria such as *S. aureus* and MRSA. The introduction of a carbazole moiety increased the strength of the antibacterial effect toward *S. aureus* ($CFU_{50}$ = 1.9–4.2 μM, $p > 37.6$), whereas the antibacterial ability was moderate toward EC-GFP and MRSA and weak toward *E. coli* and ESBL-EC ($CFU_{50}$ > 128.0 μM). The negative amino group of carbazole affects the antibacterial ability of a positively charged imidazolium salt toward Gram-negative bacteria and enhances the antibacterial ability toward Gram-positive bacteria. In sum, the imidazolium salts **DIM** and **DID** showed strong antibacterial effects ($p > 5.8$) compared to the imidazoline-2-thiones ($\mathbf{R_1SR_2}$) **DSM** and **DSD**, respectively. Thus, **DSM** and **DSD** were potentially selected for OFF-ON antibacterial fluorescent probes.

## $ClO^-$ Response

Recognition of ROS/RNS by **DSM** was observed through UV–vis absorption and fluorescence emission spectroscopy in PBS buffer with a pH value of 7.4 (0.5% DMF). The absorbance band (300–375 nm) of **DSM** (5 μM) is decreased, and its blue fluorescence emission is significantly enhanced after 30 min of incubation in $ClO^-$ (50 μM). In sharp contrast, the UV–vis absorption spectra of **DSM** are slightly changed, and its fluorescence emission is quenched upon exposure to other types of ROS/RNS, even at higher concentrations (**Figure 6A**; **Supplementary Figure S51**). On the other hand, when **DSD** (5 μM) was treated with $ClO^-$ (0–160 μM), its fluorescence emission was also inhibited (**Supplementary Figure S50A**). **DSD** cannot react to $ClO^-$ owing to steric hindrance between the two dibromobenzyl groups. Thus, **DSM** showed a highly selective response to $ClO^-$ among various ROS/RNS, relative to other $\mathbf{R_1SR_2}$ (**Figure 6A**). Upon the gradual addition of $ClO^-$ (0–65 μM) to **DSM** (5 μM) in PBS buffer with a pH value of 7.4 (0.5% DMF), the absorption band at 300–375 nm decreased, and an absorption peak appeared at about 325 nm (**Figure 7A**). Furthermore, the fluorescence intensity of **DSM** (5 μM) at ~445 nm was significantly increased in the presence of $ClO^-$ (50–65 μM) (**Figure 7A**), which is attributed to the appearance of **DIM** *via* desulfurization (**Figure 6B**). Thiourea, a basic form of $N_2C=S$, occurs in two tautomeric isomers, a thione form and a thiol form. The thiol form of **DSM** can react with reactive $ClO^-$, leading to the breakage of the C–S bond and the formation of **DIM** (**Figure 6B**). The reaction of this fused imidazolium salt was referred to in several previous reports (Xu et al., 2015; Xu et al., 2016). The conversion of **DSM** to imidazolium salt was examined *via* the reaction of **DSM** and $ClO^-$ under similar conditions. The obtained main product (**DSM′**) was confirmed with **DIM** by $^1H$ NMR, $^{13}C$ NMR, and ESI-HRMS (**Supplementary Figures S35, S36B**). Furthermore, **DSM** was highly sensitive to $ClO^-$, with a detection limit (LOD) of 0.13 μM (**Supplementary Figure S50B**), which is lower than that of many $ClO^-$ probes in previous reports (Xiao et al., 2015; Shen et al., 2017; Wang et al., 2018; Lee S. C. et al., 2020; Nguyen et al., 2020).

Owing to the high fluorescence emission quantum yield and antibacterial activity of **DIM**, **DSM** can act as a potential OFF-ON

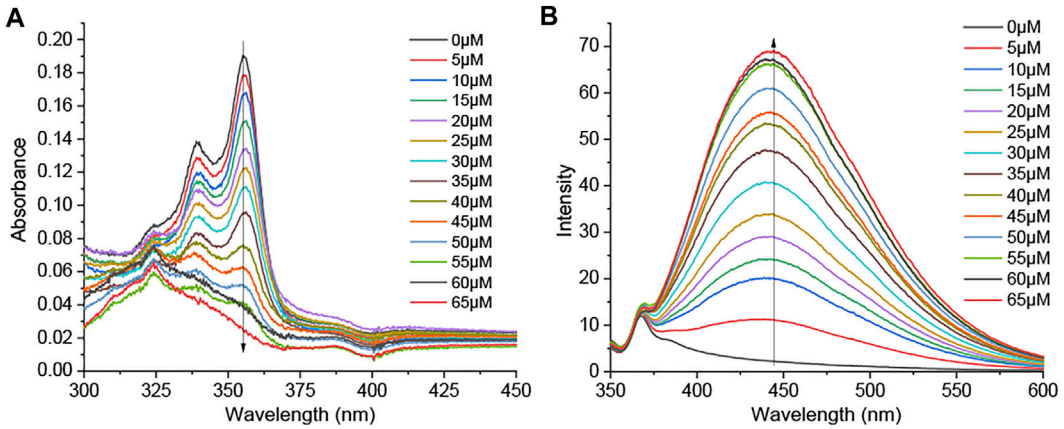


**FIGURE 7 | (A)** UV–vis absorption and **(B)** fluorescence emission spectra ($\lambda_{ex}$ = 325 nm; slit 5/5) of **DSM** (5 μM) upon treatment with $ClO^-$ (0–65 μM) in PBS with a pH value of 7.4 (0.05% DMF).

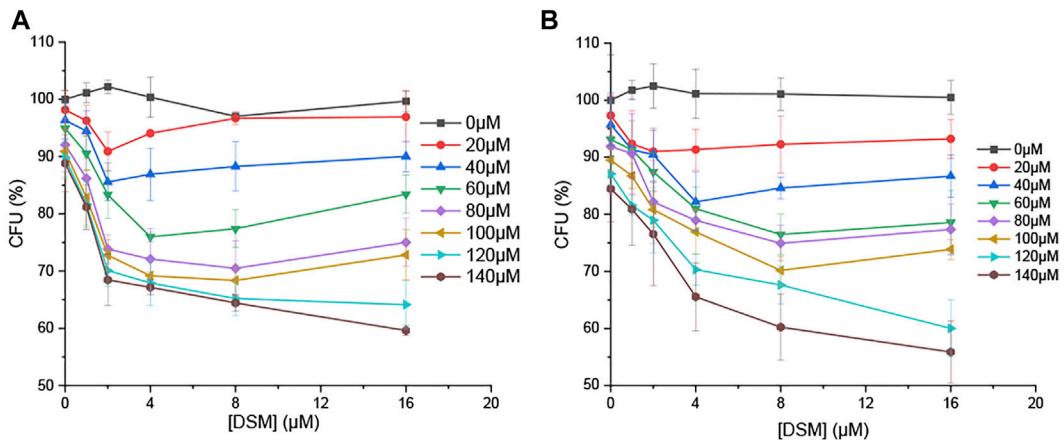


**FIGURE 8 |** CFU percentage (%) of bacteria in the presence of **DSM** (0, 1, 2, 4, 8, and 16 μM) and $ClO^-$ (0, 20, 40, 60, 80, 100, 120, and 140 μM) toward **(A)** ESBL-EC and **(B)** MRSA.

fluorescent and antibacterial probe in the presence of $ClO^-$. Consequently, it was further studied in an antibacterial test. ESBL-EC and MRSA were treated with **DSM** (0–16 μM) and/or $ClO^-$ (0–140 μM). The CFU percentage was measured after 18 h of incubation. The growth of bacteria was slightly inhibited in the presence of either $ClO^-$ (0–140 μM) or **DSM** (0–16 μM) (**Figure 8**). In contrast, their CFU percentages decreased under simultaneous treatment with $ClO^-$ and **DSM**. At $ClO^-$ concentrations of 20 and 80 μM, the lowest CFU rates were achieved at **DSM** concentrations of 2 and 8 μM, respectively. At a higher concentration of $ClO^-$ (140 μM), the lowest CFU rates were observed to be 59.6 and 55.9% at 16 μM of **DSM** toward ESBL-EC and MRSA bacteria, respectively. This demonstrates that **DSM** is converted to **DIM** upon $ClO^-$ treatment and subsequently inhibits bacterial growth. Therefore, **DSM** can be applied as a potential $ClO^-$-activated fluorophore for enhanced fluorescence emission and antibacterial activity. This finding is unprecedented with regard to previous reports of $ClO^-$ fluorescent probes (Jiao et al., 2018; Pham et al., 2021b; Kwon et al., 2021).

## CONCLUSION

A series of imidazolium salts ($\mathbf{R_1IR_2}$) and imidazoline-2-thiones ($\mathbf{R_1SR_2}$) ($R_1$, $R_2$ = methyl, dibromobenzyl, and carbazole groups) were synthesized and characterized by $^1$HNMR, $^{13}$CNMR, mass spectra, X-ray crystal structures, and DFT calculation–based molecular orbital analysis. The excitation wavelengths of the molecules were theoretically examined *via* TD-DFT with various functions and basis sets. Imidazolium salts ($\mathbf{R_1IR_2}$) without a carbazole moiety showed high fluorescence emission, whereas imidazoline-2-thiones ($\mathbf{R_1SR_2}$) exhibited weak emission. The antibacterial activities of these compounds against *E. coli*, *S. aureus*, ESBL-EC, EC-GFP, and MRSA were studied. Among these structures, **DSM/DIM** and **DID/DSD** showed high antibacterial activity ratios that would be useful for the design of OFF-ON antibacterial probes. However, **DSD** rarely reacted with $ClO^-$ due to steric hindrance, whereas **DIM** showed a high fluorescence emission quantum yield ($\Phi_F$ = 62.9%) that would be useful for bacterial imaging, and **DSM** exhibited a highly selective $ClO^-$ response with an LOD of

0.13 μM. Finally, the **DSM** probe was converted to **DIM** upon $ClO^-$ treatment and inhibited bacterial growth.

## DATA AVAILABILITY STATEMENT

The original contributions presented in the study are included in the article/**Supplementary Material**; further inquiries can be directed to the corresponding authors.

## AUTHOR CONTRIBUTIONS

TP conceived and designed the probes and calculated the DFT in the Gaussian 09 package, V-NN designed the probes, YC synthesized the probes, DK and O-SJ calculated the X-ray crystal structures, DL and HK performed the antibacterial test, ML performed the computational study, and JY, HK, and SL designed the probes and wrote the manuscript.

## FUNDING

This research was supported by the Basic Science Research Program through the National Research Foundation of Korea (NRF), funded by the Ministry of Education (no. 2017R1A6A3A04004954 for SL).

## SUPPLEMENTARY MATERIAL

The Supplementary Material for this article can be found online at: https://www.frontiersin.org/articles/10.3389/fchem.2021.713078/full#supplementary-material

## REFERENCES

Adamo, C., and Jacquemin, D. (2013). The Calculations of Excited-State Properties with Time-dependent Density Functional Theory. *Chem. Soc. Rev.* 42, 845–856. doi:10.1039/c2cs35394f

Allen, F. H., Kennard, O., Watson, D. G., Brammer, L., Orpen, A. G., and Taylor, R. (1987). Tables of Bond Lengths Determined by X-ray and Neutron Diffraction. Part 1. Bond Lengths in Organic Compounds. *J. Chem. Soc.* 2, S1–S19. doi:10.1039/p298700000s1

Bashir, M., Bano, A., Ijaz, A., and Chaudhary, B. (2015). Recent Developments and Biological Activities of N-Substituted Carbazole Derivatives: a Review. *Molecules* 20, 13496–13517. doi:10.3390/molecules200813496

Çoban, E. P., Fırıncı, R., Biyik, H., and Günay, M. E. (2017). Unsymmetrically Substituted Imidazolium Salts: Synthesis, Characterization and Antimicrobial Activity. *Braz. J. Pharm. Sci.* 53. doi:10.1590/s2175-97902017000115075

Domigan, N. M., Charlton, T. S., Duncan, M. W., Winterbourn, C. C., and Kettle, A. J. (1995). Chlorination of Tyrosyl Residues in Peptides by Myeloperoxidase and Human Neutrophils. *J. Biol. Chem.* 270, 16542–16548. doi:10.1074/jbc.270.28.16542

Duman, A. N., Ozturk, I., Tunçel, A., Ocakoglu, K., Colak, S. G., Hoşgör-Limoncu, M., et al. (2019). Synthesis of New Water-Soluble Ionic Liquids and Their Antibacterial Profile against Gram-Positive and Gram-Negative Bacteria. *Heliyon* 5, e02607. doi:10.1016/j.heliyon.2019.e02607

Gottardi, W., Klotz, S., and Nagl, M. (2014). Superior Bactericidal Activity of N -bromine Compounds Compared to Their N -chlorine Analogues Can Be Reversed under Protein Load. *J. Appl. Microbiol.* 116, 1427–1437. doi:10.1111/jam.12474

Gupta, A., Mumtaz, S., Li, C.-H., Hussain, I., and Rotello, V. M. (2019). Combatting Antibiotic-Resistant Bacteria Using Nanomaterials. *Chem. Soc. Rev.* 48, 415–427. doi:10.1039/c7cs00748e

Hryniewicka, A., Niemirowicz-Laskowska, K., Wielgat, P., Car, H., Hauschild, T., and Morzycki, J. W. (2021). Dehydroepiandrosterone Derived Imidazolium Salts and Their Antimicrobial Efficacy. *Bioorg. Chem.* 108, 104550. doi:10.1016/j.bioorg.2020.104550

Huang, R. T. W., Peng, K. C., Shih, H. N., Lin, G. H., Chang, T. F., Hsu, S. J., et al. (2011). Antimicrobial Properties of Ethoxyether-Functionalized Imidazolium Salts. *Soft Matter* 7, 8392–8400. doi:10.1039/c1sm05759f

Jeitner, T. M., Xu, H., and Gibson, G. E. (2005). Inhibition of the Alpha-Ketoglutarate Dehydrogenase Complex by the Myeloperoxidase Products, Hypochlorous Acid and Mono-N-Chloramine. *J. Neurochem.* 92, 302–310. doi:10.1111/j.1471-4159.2004.02868.x

Jiao, X., Li, Y., Niu, J., Xie, X., Wang, X., and Tang, B. (2018). Small-molecule Fluorescent Probes for Imaging and Detection of Reactive Oxygen, Nitrogen, and Sulfur Species in Biological Systems. *Anal. Chem.* 90, 533–555. doi:10.1021/acs.analchem.7b04234

Kardas, P., Devine, S., Golembesky, A., and Roberts, C. (2005). A Systematic Review and Meta-Analysis of Misuse of Antibiotic Therapies in the Community. *Int. J. Antimicrob. Agents* 26, 106–113. doi:10.1016/j.ijantimicag.2005.04.017

Kim, H. N., Lee, E.-H., Xu, Z., Kim, H.-E., Lee, H.-S., Lee, J.-H., et al. (2012). A Pyrene-Imidazolium Derivative that Selectively Recognizes G-Quadruplex DNA. *Biomaterials* 33, 2282–2288. doi:10.1016/j.biomaterials.2011.11.073

Kim, T., Zhang, Q., Li, J., Zhang, L., and Jokerst, J. V. (2018). A Gold/silver Hybrid Nanoparticle for Treatment and Photoacoustic Imaging of Bacterial Infection. *ACS Nano* 12, 5615–5625. doi:10.1021/acsnano.8b01362

Krasowska, A., and Konat, G. W. (2004). Vulnerability of Brain Tissue to Inflammatory Oxidant, Hypochlorous Acid. *Brain Res.* 997, 176–184. doi:10.1016/j.brainres.2003.09.080

Kurapati, R., Kostarelos, K., Prato, M., and Bianco, A. (2016). Biomedical Uses for 2D Materials beyond Graphene: Current Advances and Challenges Ahead. *Adv. Mater.* 28, 6052–6074. doi:10.1002/adma.201506306

Kwon, N., Kim, D., Swamy, K. M. K., and Yoon, J. (2021). Metal-coordinated Fluorescent and Luminescent Probes for Reactive Oxygen Species (ROS) and Reactive Nitrogen Species (RNS). *Coord. Chem. Rev.* 427, 213581. doi:10.1016/j.ccr.2020.213581

Ledwon, P. (2019). Recent Advances of Donor-Acceptor Type Carbazole-Based Molecules for Light Emitting Applications. *Org. Elect.* 75, 105422. doi:10.1016/j.orgel.2019.105422

Lee, S., Cheng, H., Chi, M., Xu, Q., Chen, X., Eom, C.-Y., et al. (2016). Sensing and Antibacterial Activity of Imidazolium-Based Conjugated Polydiacetylenes. *Biosens. Bioelectron.* 77, 1016–1019. doi:10.1016/j.bios.2015.10.090

Lee, S. C., Park, S., So, H., Lee, G., Kim, K.-T., and Kim, C. (2020b). An Acridine-Based Fluorescent Sensor for Monitoring ClO− in Water Samples and Zebrafish. *Sensors* 20, 4764. doi:10.3390/s20174764

Lee, S., Pham, T. C., Bae, C., Choi, Y., Kim, Y. K., and Yoon, J. (2020a). Nano Theranostics Platforms that Utilize Proteins. *Coord. Chem. Rev.* 412, 213258. doi:10.1016/j.ccr.2020.213258

Li, X., Bai, H., Yang, Y., Yoon, J., Wang, S., and Zhang, X. (2019). Supramolecular Antibacterial Materials for Combatting Antibiotic Resistance. *Adv. Mater.* 31, 1805092. doi:10.1002/adma.201805092

Li, X., Lee, D., Huang, J.-D., and Yoon, J. (2018a). Phthalocyanine-Assembled Nanodots as Photosensitizers for Highly Efficient Type I Photoreactions in Photodynamic Therapy. *Angew. Chem. Int. Ed.* 57, 9885–9890. doi:10.1002/anie.201806551

Li, X., Lee, S., and Yoon, J. (2018b). Supramolecular Photosensitizers Rejuvenate Photodynamic Therapy. *Chem. Soc. Rev.* 47, 1174–1188. doi:10.1039/c7cs00594f

Liu, L.-X., Wang, X.-Q., Zhou, B., Yang, L.-J., Li, Y., Zhang, H.-B., et al. (2015). Synthesis and Antitumor Activity of Novel N-Substituted Carbazole Imidazolium Salt Derivatives. *Scientific Rep.* 5, 1–20. doi:10.1038/srep13101

Mullen, D., and Hellner, E. (1978). A Simple Refinement of Density Distributions of Bonding Electrons. IX. Bond Electron Density Distribution in Thiourea, CS(NH2)2, at 123K. *Acta Crystallogr. Sect B* 34, 2789–2794. doi:10.1107/s0567740878009243

Nguyen, V.-N., Heo, S., Kim, S., Swamy, K. M. K., Ha, J., Park, S., et al. (2020). A Thiocoumarin-Based Turn-On Fluorescent Probe for Hypochlorite Detection and its Application to Live-Cell Imaging. *Sensors Actuators B: Chem.* 317, 128213. doi:10.1016/j.snb.2020.128213

Pak, Y. L., Park, S. J., Wu, D., Cheon, B., Kim, H. M., Bouffard, J., et al. (2018). N-heterocyclic Carbene Boranes as Reactive Oxygen Species-Responsive Materials: Application to the Two-Photon Imaging of Hypochlorous Acid in Living Cells and Tissues. *Angew. Chem.* 130, 1583–1587. doi:10.1002/ange.201711188

Pene, F., Courtine, E., Cariou, A., and Mira, J.-P. (2009). Toward Theragnostics. *Crit. Care Med.* 37, S50–S58. doi:10.1097/ccm.0b013e3181921349

Pham, T. C., Choi, Y., Bae, C., Tran, C. S., Kim, D., Jung, O.-S., et al. (2021a). A Molecular Design towards Sulfonyl Aza-BODIPY Based NIR Fluorescent and Colorimetric Probe for Selective Cysteine Detection. *RSC Adv.* 11, 10154–10158. doi:10.1039/d0ra10567h

Pham, T. C., Heo, S., Nguyen, V. N., Lee, M. W., Yoon, J., and Lee, S. (2021b). Molecular Design toward Heavy-atom-free Photosensitizers Based on the C═S Bond and Their Dual Functions in Hypoxia Photodynamic Cancer Therapy and ClO–Detection. *ACS Appl. Mater. Inter.* 13 (12), 13949–13957. doi:10.1021/acsami.0c22174

Pham, T. C., Lee, S., Kim, D., Jung, O.-S., Lee, M. W., and Lee, S. (2020). Visual Simultaneous Detection and Real-Time Monitoring of Cadmium Ions Based on Conjugated Polydiacetylenes. *ACS Omega* 5, 31254–31261. doi:10.1021/acsomega.0c04636

Popescu, R., Filimon, M. N., Vlad, D. C., Verdes, D., Moatar, A., Moise, G., et al. (2021). Antiproliferative and Antibacterial Potential of Tetrahexylammonium Bromide-Based Ionic Liquids. *Exp. Ther. Med.* 22, 1–9. doi:10.3892/etm.2021.10104

Rehmat, N., Toffoletti, A., Mahmood, Z., Zhang, X., Zhao, J., and Barbon, A. (2020). Carbazole-perylenebisimide Electron Donor/acceptor Dyads Showing Efficient Spin Orbit Charge Transfer Intersystem Crossing (SOCT-ISC) and Photo-Driven Intermolecular Electron Transfer. *J. Mater. Chem. C* 8, 4701–4712. doi:10.1039/c9tc06429j

Reinhardt, A., Horn, M., Schmauck, J. P. g., Bröhl, A., Giernoth, R., Oelkrug, C., et al. (2014). Novel Imidazolium Salt-Peptide Conjugates and Their Antimicrobial Activity. *Bioconjug. Chem.* 25, 2166–2174. doi:10.1021/bc500510c

Riduan, S. N., and Zhang, Y. (2013). Imidazolium Salts and Their Polymeric Materials for Biological Applications. *Chem. Soc. Rev.* 42, 9055–9070. doi:10.1039/c3cs60169b

Salih, N., Salimon, J., and Yousif, E. (2016). Synthesis and Antimicrobial Activities of 9H-Carbazole Derivatives. *Arabian J. Chem.* 9, S781–S786. doi:10.1016/j.arabjc.2011.08.013

Saritha, R., Annes, S. B., Saravanan, S., and Ramesh, S. (2020). Carbazole Based Electron Donor Acceptor (EDA) Catalysis for the Synthesis of Biaryl and Aryl-Heteroaryl Compounds. *Org. Biomol. Chem.* 18, 2510–2515. doi:10.1039/d0ob00282h

Shen, B.-X., Qian, Y., Qi, Z.-Q., Lu, C.-G., Sun, Q., Xia, X., et al. (2017). Near-infrared BODIPY-Based Two-Photon ClO– Probe Based on Thiosemicarbazide Desulfurization Reaction: Naked-Eye Detection and Mitochondrial Imaging. *J. Mater. Chem. B* 5, 5854–5861. doi:10.1039/c7tb01344b

Sun, W., Li, M., Fan, J., and Peng, X. (2019). Activity-based Sensing and Theranostic Probes Based on Photoinduced Electron Transfer. *Acc. Chem. Res.* 52, 2818–2831. doi:10.1021/acs.accounts.9b00340

Valls, A., Andreu, J. J., Falomir, E., Luis, S. V., Atrián-Blasco, E., Mitchell, S. G., et al. (2020). Imidazole and Imidazolium Antibacterial Drugs Derived from Amino Acids. *Pharmaceuticals* 13, 482. doi:10.3390/ph13120482

Wang, X., Min, J., Wang, W., Wang, Y., Yin, G., and Wang, R. (2018). A Novel Porphyrin-Based Near-Infrared Fluorescent Probe for Hypochlorite Detection and its Application *In Vitro* and *In Vivo*. *Analyst* 143, 2641–2647. doi:10.1039/c8an00586a

Winterbourn, C. C., Vissers, M. C., and Kettle, A. J. (2000). Myeloperoxidase. *Curr. Opin. Hematol.* 7, 53–58. doi:10.1097/00062752-200001000-00010

Wu, D., Chen, L., Xu, Q., Chen, X., and Yoon, J. (2019). Design Principles, Sensing Mechanisms, and Applications of Highly Specific Fluorescent Probes for HOCl/OCl-. *Acc. Chem. Res.* 52, 2158–2168. doi:10.1021/acs.accounts.9b00307

Xiao, H., Li, J., Zhao, J., Yin, G., Quan, Y., Wang, J., et al. (2015). A Colorimetric and Ratiometric Fluorescent Probe for ClO−targeting in Mitochondria and its Application *In Vivo*. *J. Mater. Chem. B* 3, 1633–1638. doi:10.1039/c4tb02003k

Xu, Q., Heo, C. H., Kim, G., Lee, H. W., Kim, H. M., and Yoon, J. (2015). Development of Imidazoline-2-Thiones Based Two-Photon Fluorescence Probes for Imaging Hypochlorite Generation in a Co-culture System. *Angew. Chem. Int. Ed.* 54, 4890–4894. doi:10.1002/anie.201500537

Xu, Q., Heo, C. H., Kim, J. A., Lee, H. S., Hu, Y., Kim, D., et al. (2016). A Selective Imidazoline-2-Thione-Bearing Two-Photon Fluorescent Probe for Hypochlorous Acid in Mitochondria. *Anal. Chem.* 88, 6615–6620. doi:10.1021/acs.analchem.6b01738

Xu, Q., Lee, K.-A., Lee, S., Lee, K. M., Lee, W.-J., and Yoon, J. (2013). A Highly Specific Fluorescent Probe for Hypochlorous Acid and its Application in Imaging Microbe-Induced HOCl Production. *J. Am. Chem. Soc.* 135, 9944–9949. doi:10.1021/ja404649m

Xu, Z., Kim, S. K., and Yoon, J. (2010). Revisit to Imidazolium Receptors for the Recognition of Anions: Highlighted Research during 2006-2009. *Chem. Soc. Rev.* 39, 1457–1466. doi:10.1039/b918937h

Yaqub, G., Hannan, A., Akbar, E., Usman, M., Hamid, A., Sadiq, Z., et al. (2013). Synthesis, Antibacterial, and Antifungal Activities of Novel Pyridazino Carbazoles. *J. Chem.* 2013, 8575–8576. doi:10.1155/2013/818739

**Conflict of Interest:** The authors declare that the research was conducted in the absence of any commercial or financial relationships that could be construed as a potential conflict of interest.

The handling Editor declared a past coauthorship with one of the authors, JY.